

Valproic Acid Metabolism by Cytochrome P450: A Theoretical Study of Stereoelectronic Modulators of Product Distribution

Jack R. Collins,* Debra L. Camper, and Gilda H. Loew

Contribution from the Molecular Research Institute, 845 Page Mill Road, Palo Alto, California 94304. Received July 16, 1990

Abstract: Semiempirical, molecular mechanics, and molecular dynamics calculations have been performed to theoretically examine the metabolism of 2-*n*-propylpentanoic acid (valproic acid, VPA), a widely used therapeutic agent for the control of seizure disorders, by cytochrome P450. In particular, the stereospecificity and product distribution of the hydroxylated metabolites of VPA are predicted for the P450_{cam} isozyme and compared to the experimental data from microsomal P450. Quantum mechanical results are consistent with hypothesized mechanisms for the formation of 2-*n*-propyl-4-pentenoic acid (4-ene-VPA), a hepatotoxic metabolite, by a P450-catalyzed dehydrogenation reaction. The current theoretical results suggest that differences in the binding sites between mammalian P450 isozymes and P450_{cam} may modulate the product distribution via steric interactions with the substrate.

I. Introduction

Valproic acid (2-*n*-propylpentanoic acid, VPA), Figure 1, is an important antiepileptic agent that is widely used for the treatment of a variety of both simple and complex seizure disorders.^{1,2} It is also a member of the family of simple short-chain aliphatic acids, whose esters are widely used as organic industrial solvents. These esters are easily hydrolyzed to short-chain aliphatic acids. While initially thought to be free of toxic effects, these simple acids, including VPA, have now been implicated in causing liver damage^{3,4} as well as birth defects.^{3,5,6}

Because of its therapeutic use, the possible origins of the toxicity of VPA have been the most extensively studied of all the aliphatic acids. While detailed mechanisms leading to teratogenic activity and hepatic dysfunction are not yet understood, it has been experimentally established that VPA is teratogenic and some of its metabolites are both teratogenic and hepatotoxic.^{3,4,7,8} Moreover, a single metabolite, the 4-ene-VPA (2-*n*-propyl-4-pentenoic acid), appears to be the major source of both liver damage and birth defects.^{3,9-12}

VPA is also known to be a substrate for the metabolizing heme proteins, the cytochrome P450s.³ The cytochrome P450s are a family of ubiquitous metabolizing heme proteins that function as monooxygenases. These enzymes activate molecular oxygen to form a species, thought to be a ferryl (Fe=O) like state, that inserts a single oxygen atom into a variety of organic substrates.¹³ In general, the oxidation of saturated aliphatic hydrocarbons by the P450-mediated process leads to hydroxylated products.¹³ In fact, three hydroxylated metabolites of VPA, 3-OH, 4-OH, and 5-OH

(Figure 1), have been identified and quantified in liver microsomes from phenobarbital-treated rats.¹⁴

In addition to hydroxylation reactions, the cytochrome P450s have been recently shown to catalyze novel dehydrogenation reactions.¹⁴ The dehydrogenation of lindane,¹⁵ a hexachlorocyclohexane stereoisomer, and the 6,7 desaturation reaction of testosterone¹⁶ are examples of this unusual cytochrome P450 catalyzed reaction. Quite recently, the conversion of VPA to 4-ene-VPA has been shown to be catalyzed by liver microsomal P450.^{14,17} However, the major products are still the hydroxylated VPA derivatives.¹⁴ The 4-ene-VPA metabolite has further been implicated in the inactivation of microsomal P450s by covalently binding to the enzyme,¹² mechanistically similar to 4-pentenoic acid³ and possibly other fatty acids as well. The details of the mechanism, still unknown, possibly involve covalent adduct formation with the pyrrole nitrogens of the heme unit, or possibly the further transformation of 4-ene-VPA to 3-keto-4-ene-VPA by β -oxidation producing a metabolite that could then bind irreversibly to 3-ketoacyl-CoA thiolase.¹² Therefore, molecular properties common to these mechanisms could be valuable in predicting the metabolism of these aliphatic acids and assessing their liver toxicity.

As shown schematically in Figure 2, both experimental and theoretical evidence suggests that hydroxylations by P450 take place via a two-step radical mechanism beginning with hydrogen abstraction to form a radical intermediate that rapidly recombines with an OH radical to form the hydroxylated product.¹⁸⁻²¹ However, formation of the terminal 4-ene product is less straightforward. This desaturation reaction does not involve transfer of the active oxygen atom to the substrate, which is characteristic of P450s. Instead, it corresponds to abstraction of two H atoms, which is reminiscent of the peroxidases. Careful determination of intramolecular isotope effects of deuterated VPA

- (1) Pearlman, B. J.; Goldstein, D. B. *Mol. Pharmacol.* **1984**, *26*, 83-89.
- (2) Gram, L.; Bentsen, K. D. *Acta Neurol. Scand.* **1985**, *72*, 29-139.
- (3) Di Carlo, F. J.; Bickart, P.; Auer, C. M. *Drug Metab. Rev.* **1986**, *17*, 187-220.
- (4) Kesterson, J. W.; Granneman, G. R.; Machinist, J. M. *Hepatology* **1984**, *4*, 1143-1152.
- (5) Scott, W. J., Jr.; Duggan, C. A.; Schreiner, C. M.; Collins, M. D.; Nau, H. In *Approaches to Elucidate Mechanisms in Teratogenesis*; (Welsch, F., Ed.; Hemisphere: Washington, DC, 1987).
- (6) Brown, N. A. In *Pharmacokinetics in Teratogenicity*; Nau, H., Scott, W. J., Eds.; CRC Press: Boca Raton, FL, 1987; Vol. II.
- (7) Granneman, G. R.; Wang, S. I.; Kesterson, J. W.; Machinist, J. M. *Hepatology* **1984**, *4*, 1153-1158.
- (8) Nau, H.; Loscher, W. *Epilepsia* **1984**, *25* (Suppl. 1), S14-S22.
- (9) Prickett, K. S.; Baillie, T. A. *Drug Metab. Dispos.* **1986**, *14*, 221-229.
- (10) Baillie, T. A. *Chem. Res. Toxicol.* **1988**, *1*, 195.
- (11) Rettenmeier, A. W.; Gordon, W. P.; Prickett, K. S.; Levy, R. H.; Baillie, T. A. *Drug Metab. Dispos.* **1986**, *14*, 454-464.
- (12) Porubek, D. J.; Grillo, M. P.; Baillie, T. A. *Drug Metab. Dispos.* **1989**, *17*, 123-130.
- (13) Dawson, J. H.; Eble, K. S. *Adv. Inorg. Bioinorg. Mech.* **1986**, *4*, 1-64.

- (14) Rettie, A. E.; Rettenmeier, A. W.; Howald, W. N.; Baillie, T. A. *Science* **1987**, *235*, 890-893.
- (15) Chadwick, R. W.; Chuang, L. T.; Williams, K. *Pestic. Biochem. Physiol.* **1975**, *5*, 575-586.
- (16) Nagata, K.; Liberato, D. J.; Gillette, J. R.; Sasame, H. A. *Drug Metab. Dispos.* **1986**, *14*, 559-565.
- (17) Rettie, A. E.; Boberg, M.; Rettenmeier, A. W.; Baillie, T. A. *J. Biol. Chem.* **1988**, *263*, 13733-13738.
- (18) White, R. E.; McCarthy, M.-B.; Egeberg, K. D.; Sligar, S. G. *Arch. Biochem. Biophys.* **1984**, *228*, 493-502.
- (19) Gelb, M. H.; Heimbrook, D. C.; Malkonen, P.; Sligar, S. G. *Biochemistry* **1982**, *21*, 370-377.
- (20) Sligar, S. G.; Gelb, M. H.; Heimbrook, D. C. In *Microsomes, Drug Oxidations and Drug Toxicology*; Sato, R., Kato, R., Eds.; Wiley Interscience: New York, 1982; pp 155-161.
- (21) Loew, G. H.; Collins, J. R.; Luke, B. T.; Waleh, A.; Pudzianowski, A. *Enzyme* **1986**, *36*, 54-78.

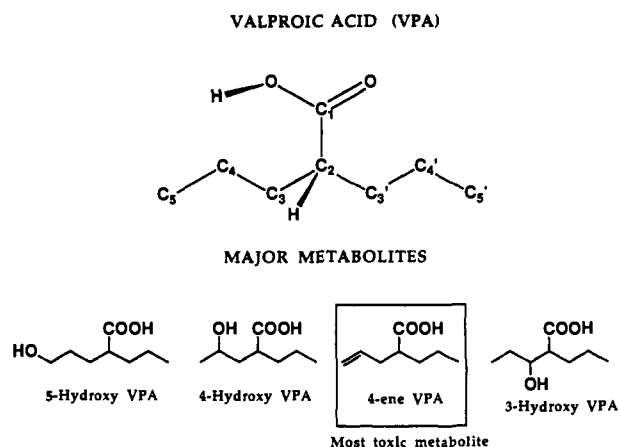


Figure 1. Valproic acid and its major metabolites.

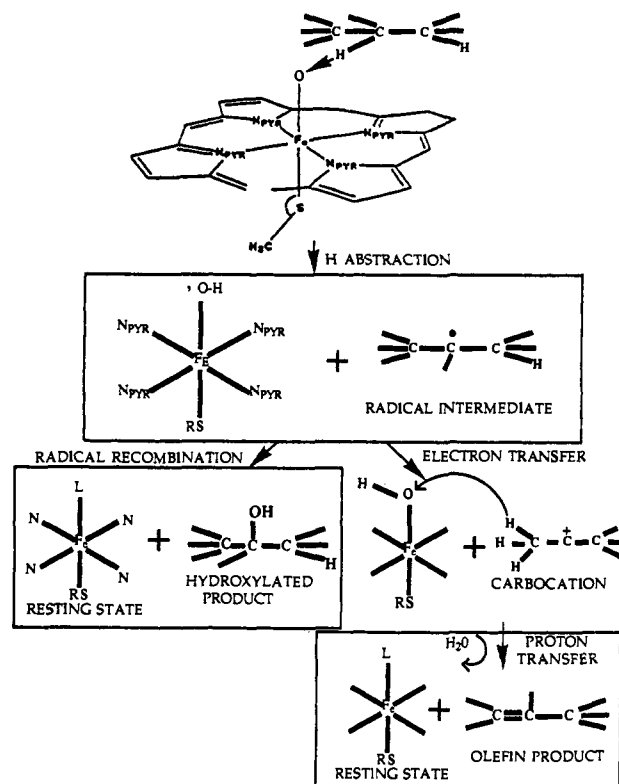


Figure 2. Proposed mechanisms of hydroxylation and olefin formation by the active ferryl state of cytochrome P450.

at the 4- and at the 5-positions on the rate of formation of the 4-OH-, 5-OH-, and 4-ene-VPA products has been reported.¹⁷ The experimental results show a marked isotope effect for the 4-ene-VPA production when 4-deuterio- but not 5-deuterio-VPA is used. This is indicative of a mechanism in which the first step is abstraction of a hydrogen from the 4-position to form the same radical intermediates as in the hydroxylation reaction. The absence of a similar isotope effect for the C5 position indicates that C4-C5 olefin formation does not proceed via H abstraction at C5, a result with no obvious explanation.

Based on the experimental isotope effects, a mechanism for the formation of the 4-ene has been proposed,^{14,22} shown schematically in Figure 2, involving H abstraction at C4 by the active ferryl oxygen of P450 leading to a C4 radical species. In competition with rapid radical recombination, it is suggested that there is an electron transfer from the C4 VPA radical to the P450-Fe-OH complex, resulting in a VPA carbocation and an Fe(OH)⁻ species.

This electron-transfer step is hypothesized to then be followed by rapid transfer of a proton from the C5 position of the VPA carbocation to the (OH⁻) forming 4-ene-VPA and water.

On the basis of these postulated mechanisms, we have calculated conformational and electronic properties of the substrate and postulated intermediates that are believed to be reliable indicators of preferred sites of both hydroxylation and olefin formation. In these calculations, we have made the assumption that valproic acid binds in its neutral form to the P450 binding site. This assumption is based on the fact that known substrates of P450s are generally hydrophobic and that the binding site itself is very lipophilic.

To characterize the parent substrate, we have performed an energy-based conformational analysis of VPA to identify its low-energy conformers. The propyl chains in VPA, while chemically equivalent, are not conformationally identical in any of the calculated low-energy conformations. These conformational differences are manifested in small differences in electronic properties in the two chains.

Since formation of both hydroxylation and olefin products appears to proceed via H abstraction, we have calculated the stability of the resulting radicals formed at each of the seven carbon atoms in VPA as a possible electronic indicator of preferred sites of formation of either type of product. Specifically, radicals formed by H atom abstraction at the three C atoms in each of the *n*-propyl chains (C3-C5 and C3'-C5') and the central carbon atom to which the carboxyl group is attached (C2) were characterized. For preferred sites of olefin formation, the calculated ionization potential of each radical was examined as a second electronic criterion, since electron donation to the heme unit has been postulated to follow radical formation. These two calculated properties constitute the candidate electronic criteria examined as modulators of preferred sites of hydroxylations and olefin formation.

To obtain possible steric modulators of product specificity, the P450_{cam} crystal structure was used to characterize VPA interactions with the binding site of the enzyme. P450_{cam}, the only P450 isozyme with a known three-dimensional structure, was used as a model for the binding site of liver microsomal P450. The steric criteria used for preferred sites of hydroxylation are the distances from the H of VPA to be abstracted to the ferryl oxygen. These distance criteria, combined with the stability of the radical at each site, are two properties found to be reliable predictors of hydroxylated product specificity in our previous studies of camphor analogue metabolism.²³ These steric criteria are also important to the preferred sites of olefin formation, also hypothesized to proceed via H abstraction.

The work reported here is the first step in an effort to develop mechanism-based structure-metabolism relationships that could aid in the assessment of the liver toxicity of aliphatic acids. If successful, the stereoelectronic criteria identified and characterized here should be able to explain the observed metabolites formed by VPA. Particularly useful would be the identification of molecular discriminants for hydroxylations versus olefin formation, the latter type leading to toxicity. These discriminants could then be used for computer-aided toxic risk assessment of other fatty acids.

II. Methods

A. Conformations of Valproic Acid. The low-energy conformations of valproic acid were calculated by using both molecular mechanics and semiempirical quantum mechanical methods. Valproic acid was first built in the extended, all-trans, conformation and optimized by use of the Quanta/CHARMm software package from Polygen.^{24,25} The single optimized starting structure was then used as the starting point for high-temperature dynamics simulations to search the conformational space for low-energy structures. Dynamics calculations were run by heating the molecule to 2000 K in 3.0 ps followed by 3.0 ps of equilibration. This step was then followed by 3.0 ps of simulation in which

(23) Collins, J. R.; Loew, G. H. *J. Biol. Chem.* **1988**, *263*, 3164-3170.

(24) Brooks, B. R.; Bruccoleri, E. R.; Olafson, B. E. R.; States, D. J.; Swaminathan, S.; Karplus, M. *J. Comput. Chem.* **1984**, *4*, 187.

(25) QUANTA 2.1 Program, Polygen Corp., Waltham, MA, 1987.

(22) Ortiz de Montellano, P. R. *Trends Pharmacol. Sci.* **1989**, *10*, 354-359.

coordinates were sampled every 0.01 ps for a total of 300 structures. Approximately 30 of the lowest energy and several randomly chosen structures were then minimized by using CHARMM. All structures within 8.0 kcal/mol of the lowest energy conformer were then optimized by the semiempirical method AM1.²⁶ Three low-energy conformers were obtained with heats of formation differing by no more than 1.0 kcal/mol from the lowest energy conformer. All other structures obtained from AM1 were at least 3.0 kcal/mol higher in energy than the minimum energy one. The barrier to rotation about the C1–C2 bond of the acid group of VPA was calculated by constraining the O–C1–C2–C3 dihedral angle at 30 °C increments while fully optimizing the rest of the molecule. The barrier of rotation was determined only for the lowest energy conformer of VPA from the dynamics search. A fourth conformer was obtained from rotating the carbonyl group, which turned out to be the lowest energy conformer located in our search.

B. Radical Formation and Ionization Calculations. The stability of each radical that could be formed by hydrogen abstraction from a carbon atom was calculated by fully optimizing the geometry of each radical starting from the lowest energy conformer of VPA using the UHF method and the AM1 Hamiltonian. Ionization potentials (IPs) were calculated in two ways. In one, Koopman's theorem was applied; i.e., the IP was approximated as the negative of the energy of the singly occupied, highest energy molecular orbital. In the second, complete geometry optimization was performed for each of the cations resulting from ionization of each of the seven radical species. The IP was then calculated as the difference in heats of formation of each cation and its parent radical (Δ SCF).

C. Enzyme–Substrate Interactions. To model the enzyme–substrate interactions of VPA with cytochrome P450, we used the binding site of P450_{cam} from the crystal structure of the adamantanone-bound enzyme.²⁷ Our binding site is composed of 87 amino acids, which forms a sphere of approximately 12 Å from the center of the heme unit.²⁸ The binding site also includes seven bound water molecules from the crystal structure and the protoporphyrin IX heme unit. Two different models of the binding site, differing in the nature of the heme unit, were used to characterize its interaction with the substrate, VPA. The first model simulated the initial binding of VPA to the enzyme. In this initial substrate-bound state, there is no second axial ligand binding to the iron and the standard porphyrin unit with modified Fe parameters was used. The second model binding site included the putative, biologically active, ferryl–oxy species. In this model, a ferryl–oxy porphyrin unit was substituted for the standard 5-coordinate Fe system. In the ferryl–oxy model, an oxygen atom was placed perpendicular to the porphyrin plane opposite from the cysteinate ligand at a distance of 1.7 Å from the Fe atom, a value consistent with that obtained for the ferryl–oxy state of peroxidases from XAFS studies.²⁹ The charges for the ferryl–oxy model (Table I) were taken from INDO/S calculations.^{30–35} Table I also gives the parameters for Fe and the ferryl oxygen used in the AMBER³⁶ calculations.

Each of the four low-energy conformers found from the AM1 calculations were docked into each binding site model of P450_{cam} in place of the adamantanone with the program MIDAS³⁷ with the X-ray structures from both camphor and adamantanone complexes serving as guides. The main orienting interaction found for these substrates, the electrostatic recognition of the Tyr96–OH group by the carbonyl group of VPA, was retained. The charges for VPA were taken from the average of the AM1 Mulliken population analyses for the two lowest energy structures. For both binding site models, two different orientations of each conformer were found in which a hydrogen bond could be formed between the

Table I. Parameters Used in AMBER Calculations for Valproic Acid and the Ferryl Heme Unit^a

Valproic Acid Charges Taken from AM1 Mulliken Populations			
atom	charge	atom	charge
C5	-0.205	C5Hs	0.08
C4	-0.16	H41	0.09
		H42	0.07
C3	-0.16	H31	0.09
		H32	0.10
C2	-0.15	H21	0.13
C1	0.30	O	-0.3
OH	-0.28	HO	0.225
C3'	-0.16	H3'1	0.09
		H3'2	0.08
C4'	-0.16	C4'Hs	0.08
C5'	-0.21	C5'Hs	0.07

Bond Parameters Added to AMBER for Heme		
	<i>k</i> , kcal/Å ²	<i>re</i> , Å
Fe–S	200	2.20
C _β –S	222	1.81
Fe–O	200	1.70

Angle Parameters Added to AMBER for Valproic Acid and Heme		
	<i>k</i> , kcal/Å ²	<i>θ</i> , deg
C2–C1–OH	70.0	120.0
C2–C1–O	80.0	120.0
O–C1–OH	80.0	120.0
C _β –S–Fe	150.0	109.0
S–Fe–N	40.0	98.0
C _α –C _β –S	50.0	109.0
N–Fe–O	50.0	90.0
S–Fe–O	10.0	180.0

Nonbonded Parameters Added to AMBER for Heme		
	<i>re</i> , Å	<i>k</i> , kcal/mol
S _{ferryl}	2.0	0.2
O _{ferryl}	1.65	0.15
Fe	0.95	0.20

Ferryl Model Charges Used for AMBER Calculations			
atom	charge	atom	charge
FE	1.5		
S	-0.65	O _{ferryl}	-0.6
C _β propionate	-0.1	C _γ propionate	0.3
C _{arom. heme}	0.15	N _{pyrrole}	-0.4

^a Heme atoms not listed were set to zero.

carbonyl group of VPA and the hydroxyl group of TYR96. In one type of orientation, (a, Tables IV and V) a linear Tyr96–OH...O=C (VPA) bond was obtained. In the other orientation (b, Tables IV and V), a bifurcated H bond in which the Tyr–OH interacts with both the carbonyl and hydroxyl oxygen of VPA was formed. As a consequence of the different hydrogen-bonding geometries, the orientations differed by a rigid rotation of the substrate molecule in a manner such that a different *n*-propyl chain of VPA was closer to the Fe=O moiety in a compared to b. Thus, eight different substrate-binding site geometries for the 5-coordinate binding site model were obtained. These complexes were then used as the starting coordinates for energy optimization using the empirical energy program AMBER.³⁶ Eight initial geometries were also obtained for the ferryl model using the same guidelines as those used for the 5-coordinate model. In addition to the use of initial geometries obtained by docking VPA into the ferryl form directly, optimized VPA complexes with the ferryl state of the binding site were also obtained by a second procedure. In this second procedure, an oxygen atom was added to the Fe of the eight optimized 5-coordinate models and the enzyme–substrate complexes reoptimized. This latter process was designed to more closely simulate the steps in the enzymatic cycle in which substrate binds before oxygen. In all, 8 5-coordinate model and 16 ferryl model geometries were optimized.

All minimizations were performed using a constant dielectric of 1.0 and a 9.0-Å cutoff distance for nonbonded interactions. The minimizations were considered to be converged when the root-mean-square gradient fell below 0.1. Because the 87 amino acids forming the extended substrate binding site were not contiguous in the protein, we constrained all backbone (N, C_α, C) atoms in coordinate space using a harmonic

(26) Dewar, M. S. J.; Zebisch, E. G.; Healy, E. F.; Stewart, J. J. P. *J. Am. Chem. Soc.* **1985**, *107*, 3902.

(27) Poulos, T. L., unpublished results.

(28) Collins, J. R.; Loew, G. H. *Int. J. Quantum Chem., Quantum Biol. Symp.*, in press.

(29) Chance, B.; Powers, L.; Ching, Y.; Poulos, T.; Schonbaum, G. R.; Yamazaki, I.; Paul, K. G. *Arch. Biochem. Biophys.* **1984**, *235*, 596–611.

(30) Edwards, W. D.; Weiner, B.; Zerner, M. C. *J. Am. Chem. Soc.* **1986**, *108*, 2196–2204.

(31) Edwards, W. D.; Zerner, M. C. *Theor. Chim. Acta* **1987**, *72*, 347–361.

(32) Ridley, J.; Zerner, M. *Theor. Chim. Acta* **1973**, *32*, 111–134.

(33) Ridley, J.; Zerner, M. *Theor. Chim. Acta* **1976**, *42*, 223–236.

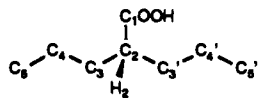
(34) Bacon, A. D.; Zerner, M. C. *Theor. Chim. Acta* **1979**, *53*, 21–54.

(35) Zerner, M. C.; Loew, G. H.; Kirchner, R. C.; Mueller-Westerhoff, U. T. *J. Am. Chem. Soc.* **1980**, *102*, 589–599.

(36) Singh, U. C.; Weiner, P. K.; Caldwell, J. W.; Kollman, P. A. AMBER UCSF Version 3.0a, Dept. of Pharmaceutical Chemistry, University of California, San Francisco, 1986.

(37) Ferrin, T. E. The MIDAS Display System. *J. Mol. Graphics* **1988**, *6*, 13–27.

Table II. Calculated Heats of Formation and Torsional Angles for Four Lowest Conformers

compound	conformers	H_f , kcal/mol	torsional angles, ^a deg						
			τ_1	τ_2	τ_3	τ_4	τ_5	τ_6	τ_7
	VPA(4)	-133.2	179.0	54.3	-71.4	96.3	-81.0	179.7	-19.7
	VPA(3)	-133.3	175.4	66.6	-57.2	112.1	-173.7	179.9	-5.6
	VPA(2)	-133.7	178.5	-175.4	62.2	-11.6	-173.6	172.7	-129.6
	VPA(1)	-134.2	-178.5	-154.3	83.1	127.4	-168.6	-175.8	8.9

^aTorsional angles are defined as follows: $\tau_1 = C_5-C_4-C_3-C_2$, $\tau_2 = C_4-C_3-C_2-C_1$, $\tau_3 = C_4-C_3-C_2-C_3'$, $\tau_4 = C_3-C_2-C_1-O$, $\tau_5 = C_3-C_2-C_3'-C_4'$, $\tau_6 = C_2-C_3-C_4-C_5$, $\tau_7 = O-C_1-C_2-H_2$.

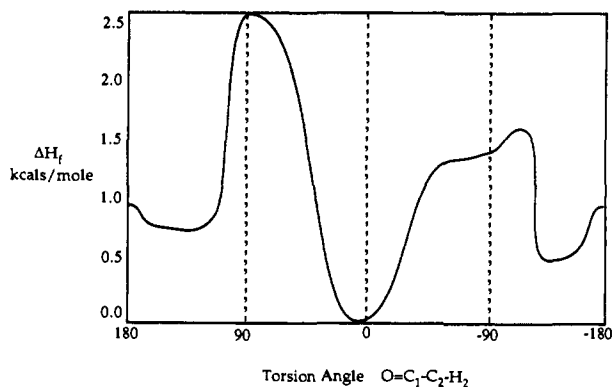


Figure 3. Rotational energy profile of the carboxy group about the C1-C2 bond in valproic acid calculated by the AM1 method.

potential of 100 kcal/Å² in all of the molecular mechanics calculations. All side-chain, porphyrin, and substrate molecules were allowed to move freely.

Net intermolecular energies between the protein binding site and the substrate were calculated with the ANAL program from AMBER. The Fe=O...HC(VPA) distances for the ferryl-state heme model were calculated from distances found in the optimized VPA binding site complexes.

Finally, molecular dynamics (MD) simulations of 40 ps preceded by 5 ps of heating and equilibration were performed using the same energy functions and harmonic potentials as described for the minimizations. The temperature was held constant at 298 K by using a coupling parameter of 0.1, and the SHAKE procedure was used to constrain all bond lengths during the simulation. Two qualitatively different orientations for the ferryl model were used as the starting geometries for the MD simulations, VPA1a and VPA2a. All statistics, such as average distances from the hydrogen atoms of VPA to the ferryl oxygen, and their standard deviations, were calculated from coordinates saved every 0.25 ps during the 40-ps simulation.

III. Results

The energy conformational studies of VPA led to the identification of four low-energy structures within 1 kcal/mol of our lowest energy, AM1 optimized, conformer. The torsion angle values and relative energies of these conformations are given in Table II. The major difference between the two lowest substrate conformations (VPA1 and VPA2) is the orientation of the acid group with respect to the rest of the molecule. VPA1 has an O-C1-C2-H2 torsion angle of 9°, while that for VPA2 is -130°. The barrier to rotation was determined for the surface leading from VPA1 to VPA2 with the results shown in Figure 3. The results indicate a barrier of less than 2 kcal/mol to rotate this torsion angle from its value in VPA1 to VPA2. Therefore, either of these two conformers, and even the two higher energy conformers (VPA3, VPA4), which are less than 1 kcal/mol from the minimum-energy one, could be energetically accessible in the binding site of P450, in the absence of additional steric factors imposed by the protein. These four conformers were chosen to model the enzyme-substrate interactions with the P450_{cam} binding site.

The heats of formation of the radicals formed by abstracting a hydrogen atom from each of the seven possible positions in VPA, yielding a carbon radical, were calculated for the two lowest energy

Table III. Valproic Acid, Radicals and Cations: Heats of Formation and Ionization Potentials from AM1 Optimized Geometries

radical	H_f (radical), kcal/mol	H_f (cation), kcal/mol	IP1, ^a eV	IP2, ^b eV
R5 (VPA1)	-101.0	102.2	9.6	8.8
R4 (VPA1)	-106.3	56.0	9.3	7.1
R3 (VPA1)	-105.6	90.3	9.6	8.5
R2 (VPA1)	-107.7	94.2	9.8	8.8
R3' (VPA1)	-105.6	87.9	9.6	8.4
R4' (VPA1)	-106.0	56.5	9.2	7.1
R5' (VPA1)	-100.1	94.0	9.6	8.4
R5 (VPA2)	-100.5	102.1	9.4	8.8
R4 (VPA2)	-106.2	85.8	9.1	8.3
R3 (VPA2)	-105.1	90.5	9.3	8.5
R2 (VPA2)	-108.4	94.2	9.9	8.8
R3' (VPA2)	-105.0	90.3	9.6	8.5
R4' (VPA2)	-105.6	56.5	9.2	7.1
R5' (VPA2)	-99.6	94.1	9.7	8.4

^aIP1, Vertical IP from Koopman's theorem. (E_{HOMO} , energy of highest occupied molecular orbital). ^bIP2, Δ SCF difference in calculated heat of formation of a neutral radical and cation.

conformers of VPA (VPA1, VPA2) and are given in Table III. Total geometry optimization was performed for each radical. Comparisons of these geometries with the parent indicated that there is no significant difference, except in the carbon atom from which the H was abstracted. The geometry of this carbon atom is altered from tetrahedral to planar and the unpaired electron is localized on it.

The heats of formation of the seven carbocations resulting from ionization of each of the seven radical species were also calculated (Table III). All carbocation geometries were fully optimized. From these calculations, a second value of the ionization potential (IP2) was calculated as the difference in energy of the radical and its cation and is also given in Table III. The geometries of the optimized cations were, in general, very similar to that of the radical species from which they were formed. However, when a carbocation is formed at C4 or C4' in the lowest energy conformer (VPA1), or at C4' in VPA2, there is a significant geometry rearrangement and an internal H-bonded, five-membered, protonated lactone is formed. As seen in Table III, this lactone is a very stable cationic species, 30–46 kcal/mol more stable than any of the unrearranged carbocation species.

When each of the four low-energy conformers of VPA (VPA1-4) are "docked" into the substrate binding site of the 5-coordinate ferric P450_{cam}, there are two possible orientations that retain the electrostatic recognition of the Tyr96-OH group by the carbonyl group of VPA. The energies of interaction of these eight optimized VPA-binding site complexes, along with the van der Waals and electrostatic/H-bonding contributions, are given in Table IV. In one of these orientations, called the "a" orientation, a linear H bond was formed between the Tyr-OH and the carbonyl oxygen of VPA, very similar to that formed by camphor, adamantanone, and other substrates of this type. In the other, called the "b" orientation, the Tyr-OH formed a bifurcated H bond with the carbonyl and hydroxyl oxygen of the VPA, an option not possible with the camphor-like analogues, which have only one oxygen group.

Table V lists the intermolecular energy decomposition between VPA and the protein for all of the ferryl-oxy complexes. The

Table IV. Intermolecular Interaction Energies^a of the Eight Minimized Substrate-Bound Ferric P450 Complexes

E-S complex	E_{VDW}^b	$E_{ES/H\ bond}^c$	$E_{int\ substr}^d$	E_{total}
VPA1a	-17.18	-5.25	4.50	-17.93
VPA1b	-15.01	-10.37	7.45	-17.93
VPA2a	-18.15	-8.96	3.25	-23.86
VPA2b	-14.93	-7.33	5.19	-17.07
VPA3a	-17.34	-5.46	6.52	-16.28
VPA3b	-14.46	-8.94	6.52	-16.88
VPA4a	-15.17	-6.24	4.03	-17.38
VPA4b	-16.46	-6.21	3.47	-19.20

^aAll energies are in kilocalories per mole. ^bVan der Waals, dispersion contribution to interaction energy. ^cElectrostatic/H bond energy contribution to total energy. ^dInternal substrate energy.

Table V. Intermolecular Interaction Energies of the Minimized Substrate-Bound Ferryl P450 Complexes

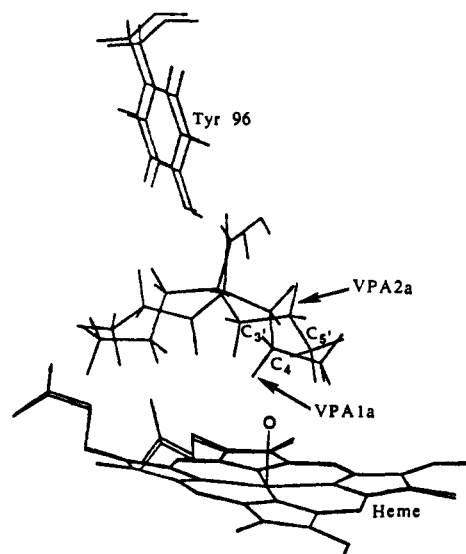
	VDW	$E_{ES/H\ bond}$	$E_{int\ substr}$	E_{total}
(I) Substrate-Bound Ferryl State from Optimized Substrate-Bound Ferric State				
VPA1a	-17.44	-7.31	3.99	-20.76
VPA1b	-16.25	-11.14	7.11	-20.38
VPA2a	-17.98	-10.12	3.64	-24.47
VPA2b	-12.57	-9.58	5.80	-16.35
VPA3a	-15.03	-7.54	3.99	-18.58
VPA3b	-15.83	-10.87	6.75	-19.95
VPA4a	-14.76	-8.58	5.63	-17.71
VPA4b	-14.39	-3.24	5.42	-12.21
(II) Substrate-Bound Ferryl State Optimized Directly				
VPA1a	-17.12	-7.42	4.12	-20.42
VPA1b	-13.48	-10.93	5.47	-18.94
VPA2a	-17.23	-9.69	3.98	-22.94
VPA2b	-16.02	-7.78	8.85	-14.95
VPA3a	-17.20	-10.16	4.97	-22.39
VPA3b	-14.99	-8.61	3.52	-20.08
VPA4a	-16.10	-7.55	6.27	-17.38
VPA4b	-13.23	-10.02	7.33	-15.92

Table VI. Average Distances of H Atoms in VPA to the Ferryl Oxygen Atom in P450_{cam}

H atom	Boltzmann weighted $r(FeO-H)$, Å	dynamics $\langle r \rangle$ (+SD), Å	
		VPA2a	VPA1a
C5(1)	5.7	5.9 (0.7)	3.7 (1.0)
C5(2)	6.3	5.5 (0.6)	4.3 (0.5)
C5(3)	6.4	6.2 (0.4)	3.7 (0.8)
C4(1)	4.0	5.2 (1.1)	3.2 (1.1)
C4(2)	4.0	4.5 (0.8)	3.9 (0.6)
C3(1)	5.9	4.8 (0.9)	3.9 (0.7)
C3(2)	5.7	5.6 (0.3)	2.9 (0.4)
C2	4.3	4.4 (0.3)	4.6 (0.6)
C3'(1)	4.1	4.0 (0.3)	5.7 (0.7)
C3'(2)	2.5	2.6 (0.2)	4.5 (0.5)
C4'(1)	3.6	3.6 (0.4)	6.7 (0.3)
C4'(2)	4.7	4.7 (0.2)	6.5 (0.4)
C5'(1)	4.2	4.1 (0.3)	5.5 (1.1)
C5'(2)	3.6	3.3 (0.5)	5.3 (0.6)
C5'(3)	2.5	2.8 (0.7)	6.2 (0.6)

table is divided into two sections; I, which lists results obtained when the ferryl oxygen atom is added to the minimized 5-coordinate geometries, and II, which lists those obtained when the VPA substrate molecule was docked into the binding site with the ferryl oxygen already in place. Also listed in Table V are the AMBER-derived intramolecular energies of the substrate as minimized in the 16 binding site-substrate ferryl complexes. The distances from the ferryl oxygen to each H atom, in these 16 different optimized VPA-ferryl binding site complexes were calculated, and along with the corresponding energies from Table V, were used to calculate a Boltzmann-weighted, energy average, distance, which is given in Table VI.

Molecular dynamics simulations of 40 ps were run, starting from the minimized enzyme-substrate complexes, VPA1a and VPA2a, shown in Figure 4. Table VI lists the average distances from

**Figure 4.** Minimized orientations of valproic acid conformers VPA1a and VPA2a in the binding site of cytochrome P450_{cam}.**Table VII.** Number of MD Snapshots within Ranges Shown for the MD Simulations of VPA in Cytochrome P450_{cam}

H atom	distance from H atoms to the ferryl O					
	<2.7 Å		≥2.7 and ≤3.5 Å		>3.5 Å	
	VPA2	VPA1a	VPA2a	VPA1a	VPA2a	VPA1a
C5'(1)	114	0	17	0	28	160
C5'(2)	26	0	62	0	71	160
C5'(3)	1	0	10	0	148	160
C4'(1)	0	0	0	0	159	160
C4'(2)	1	0	49	0	109	160
C3'(1)	126	1	34	10	0	149
C3'(2)	0	0	19	0	140	160
C2(1)	0	0	0	1	160	159
C3(1)	0	49	0	99	160	12
C3(2)	0	4	7	46	153	110
C4(1)	0	13	5	22	155	125
C4(2)	0	96	2	19	158	45
C5(1)	0	27	0	42	160	91
C5(2)	0	0	0	7	160	153
C5(3)	0	46	1	32	159	82

the 40-ps MD trajectories, along with their corresponding standard deviations. A more detailed analysis of the MD simulations grouped the Fe=O...HC(VPA) distances into three regions: (1) <2.7 Å, (2) between 2.7 and 3.5 Å, and (3) >3.5 Å. The distances were selected based on the van der Waal's radii for the H and O atoms used in the molecular mechanics calculations. The first region is assumed to be the most probable for H abstraction while the third region is expected to be unreactive. The second region is not expected to be as probable for H abstraction as the first region, but we cannot rule these out with complete confidence. These results, listed in Table VII, give the total number of MD "snapshots" with Fe=O...HC(VPA) distances found within each of the three regions that correspond to decreasing probabilities for H abstraction.

IV. Discussion

The enzymatic metabolism of VPA by microsomal cytochrome P450 results in the hydroxylated products 4-OH-, 3-OH-, 5-OH-, and 4-ene-VPA in decreasing amounts.¹⁴ The formation of the hydroxylated metabolites has been demonstrated to proceed through a radical mechanism from the large intra- and intermolecular deuterium kinetic isotope effects.¹⁷ The most likely first step is the abstraction of a hydrogen atom from the substrate by the ferryl-oxygen species resulting in a free radical. This process can then be followed by rapid radical recombination to form the hydroxylated product. Since no barrier is expected for radical recombination, the stability of the resulting radical should

be directly related to the ease of the abstraction of the hydrogen atom. Thus, the stability of the VPA radicals is one electronic property that has to be considered in determining the product distribution of the hydroxylated species. Using the results in Table III, and this criterion only, we would expect to find 2-OH > 4-OH > 3-OH > 5-OH with the amount of 4- and 3-hydroxy products being very similar. The absence of the 2-OH product from the experimentally determined product distribution suggests, however, that the formation of the hydroxylated metabolites is not determined solely by electronic factors. This fact is not unexpected, however, based upon earlier studies showing that steric factors in the protein-substrate complex play a significant role in the product distribution of camphor and its analogues.²³

The experimentally observed olefin formation in microsomal P450 is also hypothesized to proceed via H atom abstraction followed by electron transfer from the radical to the heme unit. Thus, the ionization potential of the resulting radical species may be a discriminating factor in the site and ease of olefin formation. From Table III, we see that the radical formed at C4 has the lowest ionization potential as calculated by two different methods. Therefore, consistent with experimental observation, terminal olefin formation at each *n*-propyl chain via a C4, C4' carbocation intermediate is predicted. The higher vertical ionization potential (IP1) of the C5, C5' radical can also explain why the terminal olefin is formed preferentially via the C4 radical species, as shown by the kinetic isotope studies. These results support the previously proposed mechanism of olefin formation²² and also explain the preferred reaction site, based on the electronic properties of the radical species. The much lower heats of formation for the geometry-optimized C4 and C4' cations in Table III are due to a significant change in structure of these species. In the absence of the protein environment, the final products from ionization of the radicals at C4 and C4' are predicted to be cyclic lactone structures. Even though lactones have been observed as metabolites of VPA,¹⁰ we cannot state that the reported products were formed in the enzyme binding site as opposed to acid-catalyzed dehydrolysis of the hydroxy species in solution.

Therefore, if we compare the product distribution of VPA oxidized by P450 with the calculated electronic properties of the substrate only, we would predict the trend seen from experiment with the exception of the C2 metabolite. Thus, although electronic criteria alone incorrectly predict the C2-OH product to be the most abundant, they provide a consistent rationale for the relative abundance of the hydroxylated products and also suggest a plausible pathway for the preference of olefin formation proceeding via H abstraction at the C4 and C4' positions of VPA.

In spite of the relative success of the electronic criteria in explaining the product distribution of VPA metabolized by P450, from the experimental evidence and previous studies, it is also likely that the steric constraints imposed on VPA by the protein play a significant role in the product distribution of the hydroxylated species. Examination of the sequence homology of these 87 amino acids in P450_{pb-4}, a major isozyme of microsomal P450s, and P450_{cam} revealed a large percent of similar types of amino acids, giving hope that the results using P450_{cam} to deduce steric factors are applicable to the binding and metabolism of VPA by microsomal P450s. Even though there are differences between the binding sites of P450_{cam} and microsomal P450s, we believe that our binding site model should be qualitatively similar to microsomal isozymes since each bind and metabolize similar substrates. Specifically, the two substrates, valproic acid and camphor, the natural substrate for P450_{cam}, are structurally similar in that (1) each has a carbonyl group that can bind to a residue with a hydrogen-bonding side chain such as the Tyr96 hydroxyl group, (2) they are largely lipophilic, and (3) they are approximately the same size. The molecular volumes of camphor and valproic acid are ~156 and ~149 Å³, respectively. The calculated molecular volumes of the different conformations of VPA differed by no more than 3 Å³.

The role of steric factors in modulating product specificity in VPA metabolism by P450 is complicated by the conformational flexibility of VPA, having at least four low-energy conformers

that are able to bind in two qualitatively different orientations in the P450_{cam} binding site. From Table IV we see that each of the starting orientations of the valproic acid substrate can assume a conformation that forms a stable complex with the resting-state protein. However, it is not clear to what extent subsequent binding of oxygen will affect these conformations and orientations of the substrate in the initial binding. To investigate this, the geometries of the substrates were reoptimized in the ferryl model of the protein in two different ways resulting in the energies listed in Table V, which include the internal energy of the substrate and a relative energy ordering based on the total energy of the system, assuming the protein energy to remain relatively constant. Small changes in the energy orderings due to the steric constraints imposed by the oxygen atom in the ferryl model, which would also be present in the active state of the enzyme, are seen from Tables IV and V.

The Fe=O...HC(VPA) distances were calculated for each of the ferryl-VPA complexes along with the sum of the inter- and intramolecular VPA energies. Combining the energies with the distances, we calculated Boltzmann-weighted average distances for the Fe=O...HC(VPA) interactions, listed in Table VI. Using these calculated distances, we find that the C2-H is too distant from the oxygen atom for H abstraction. The reason for the absence of the C2-OH product is even more evident from the MD results listed in Table VII. This steric constraint, due to the hydrogen bond formed between the acid group of VPA and the hydroxyl group of Tyr96, explains why there is no C2-OH product observed even though we predict the most stable radical to be formed at this site. On the basis of these results, we would predict that the hydroxylated products of VPA metabolized by P450_{cam} would be dominated by the C3' and C5' species. Combining this with the electronic criteria, we would expect the C3' hydroxy species to be the major product followed by C5' and very little, if any, C4'-OH, C4-OH, C5-OH, C3-OH, or 4-ene. These results suggest that the products will be stereoselective at the C2 chiral center, strongly favoring the C2 *S* configuration. Further stereoselectivity may also be found at the second chiral center formed in the case of the C3' hydroxy product. If the orientation of the radical is the same as in our calculations, we would expect the stereochemistry to be *R* about the chiral center at C3'.

To investigate the role of dynamic flexibility in determining the most probable hydrogens to be abstracted, we performed molecular dynamics simulations on two ES complexes in which VPA is in qualitatively different orientations (VPA2a and VPA1a). These two were chosen because they were the two lowest energy complexes for the particular types of VPA orientations in which one *n*-propyl chain is closer to the oxygen, leading us to expect hydroxylated products at C3' and C5' (VPA2a), and another in which metabolism at C4 (VPA1a) would be possible. Table VI lists the MD average distances, along with their standard deviations, for the two different 40-ps simulations. In agreement with the Boltzmann averaged distances, the average MD results starting from the lowest energy structure (VPA2a) suggest that the C3' and C5' hydroxylated products would predominate. Consistent with the average MD results for VPA2a, we see from Table VII that only the C3' and C5' hydrogens approach within 2.7 Å of the ferryl oxygen for a significant fraction of the MD simulation. Figure 5 shows the time course for the distance fluctuation for C3' and C5' hydrogens from the MD simulations of VPA2a. These distances show only minor fluctuations for the C3' hydrogen while the C5' hydrogen displays a large increase in its distance after 30 ps. This large increase in distance is due to a rotation of the methyl group and can be seen to be replaced by a second C5' hydrogen from the results listed in Table VII. Thus, the movement of the C3', C4', and C5' hydrogen atoms of VPA in the VPA2a dynamics simulation is quite restricted. On the basis of all of these criteria, we predict that the major metabolites by VPA by P450_{cam} would be C3' and C5' hydroxylated products, which are stereoselective about the C2 carbon with the *S* stereoisomer dominating.

In contrast to the unambiguous results obtained from the MD simulation starting from the lowest energy ES complex, those

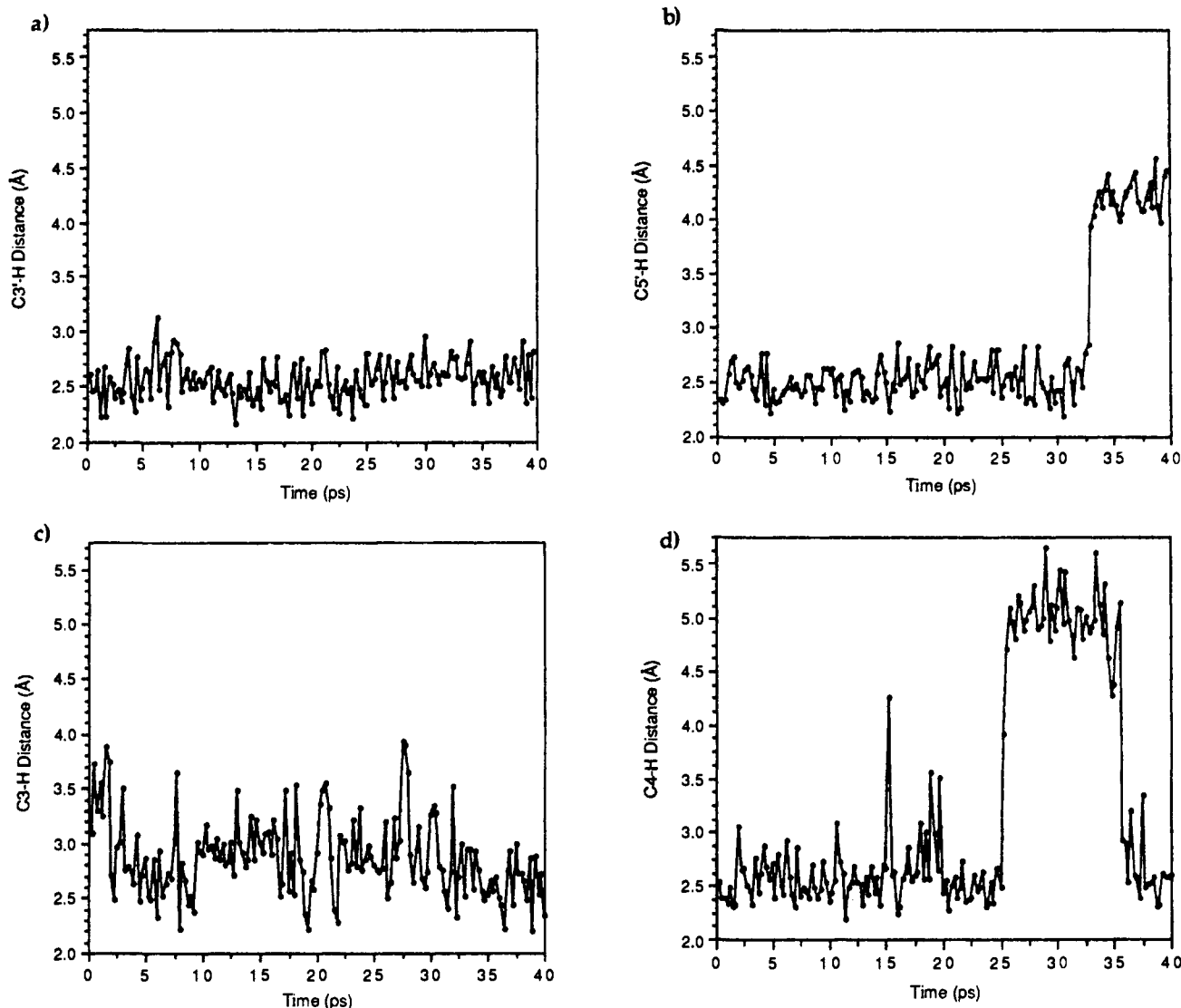


Figure 5. Plot of $\text{Fe}=\text{O}\cdots\text{HC}(\text{VPA})$ distances as a function of simulation time for (a) $\text{C3}'\text{-H}$ and (b) $\text{C5}'\text{-H}$ for the simulation of VPA2a, and (c) C3-H and (d) C4-H for the simulation of VPA1a from 40 ps of molecular dynamics.

starting from the VPA1a structure resulted in much more fluctuation of the substrate in the binding site. In this simulation, the chain favoring the *R* stereoisomer was nearer to the ferryl oxygen. As can be seen from Tables VI and VII, the C4 hydrogens are closer to the ferryl oxygen a greater fraction of the time, compared to C5 and C3. However, as seen from Figure 5, there are much larger deviations in the ferryl distances to the two closest hydrogens than found in the MD simulation starting from VPA2a. Further, Figure 5 shows a structural change between 25 and 35 ps, illustrated by the increased $\text{C4-H}\cdots\text{O}=\text{Fe}$ distance. This change demonstrates that two conformations of the substrate are in dynamic equilibrium when the simulation is started from VPA1a. Because of this increased flexibility, the predicted hydroxylation products from this trajectory are less clear than those from the VPA2a simulation. However, we might expect to see C4-OH and C3-OH products with the possibility of some C5-OH if the VPA1a starting geometry is energetically accessible in the binding site of P450.

Combining the results of all of these calculations, we would predict that the order of hydroxylated products for VPA with P450_{cam} could be $\text{C3}'\text{-OH} + \text{C3-OH} > \text{C5}'\text{-OH} \geq \text{C4-OH}$. Thus, the main modification of predicted metabolites introduced by considering dynamic behavior, assuming all conformations and orientations to be equally accessible, is a reduction in the stereoselectivity of C3-OH hydroxylation and the possible formation of some C4-OH product with the reverse (*R*) stereoselectivity at the C2 chiral center. Significantly, in none of these calculations

is $\text{C4}'\text{-OH}$ predicted to be a significant product from the metabolism of VPA with cytochrome P450_{cam} . As a consequence of this stereoselectivity and the dependence of the dehydrogenation reaction on C4-H abstraction, we would predict that only the *R* isomer of the 4-ene VPA would be found in detectable amounts.

The experimental results from metabolism of VPA by microsomal P450s are in the order $\text{C4-OH} > \text{C3-OH} > \text{C5-OH}$,¹⁴ with no reported identification, as yet, of the stereoselectivity of product formation. The greatest disparity between the results obtained here, based on the P450_{cam} binding site, and those found experimentally for microsomal P450 is our prediction of less C4 metabolite due to steric constraints imposed by the binding site. This result is an important difference since C4-OH is the major product when VPA is metabolized by microsomal P450s and hydrogen abstraction at the C4/C4' carbon is the first step in the formation of the toxic 4-ene.

There are several possible origins for the difference between the experimental data for microsomal P450 and our predicted metabolites using P450_{cam} as a model. The most probable is that the binding sites of P450_{cam} and the microsomal P450 isozymes are somewhat different. Thus, quantitative differences between the product distributions could easily be due to relatively minor differences in the steric constraints imposed by the binding sites of the two isozymes. For example, a small change in binding site architecture in microsomal P450 could allow both qualitatively different orientations to bind with more equivalent or even reversed binding energies. This could account for the predominance of the

C4-OH product seen in the microsomal P450s.

Predicted stereoselective product formation from VPA metabolism by P450_{cam} could be checked by performing experiments using VPA as the substrate, with P450_{cam} as the enzyme instead of microsomal P450s. If the results are consistent with those predicted by our calculations, the methods used here to predict the metabolites of P450_{cam} would be validated. We would then conclude that the differences in product distribution between P450_{cam} and microsomal P450 are, in fact, due to specific isozyme differences. These experiments are now in progress.³⁸

V. Conclusion

From our calculations of the electronic properties of valproic acid and the protein-substrate interactions of VPA with cytochrome P450_{cam}, we have given a reasonable explanation for the observed 4-ene product based upon an initial hydrogen abstraction at the C4 or C4' positions and made predictions for the site and stereospecificity of the hydroxylated metabolites from P450_{cam}. In particular, we have predicted that the metabolites from reaction with P450_{cam} should yield stereospecifically hydroxylated products with C3'-OH + C3-OH > C5'-OH ≥ C4-OH. The predicted product distribution is in contrast to the experimental findings of C4-OH > C3-OH > C5-OH for microsomal P450s, although the stereospecificities of the metabolites of microsomal P450 have not been determined. If our calculated results are correct for P450_{cam}, we would have to conclude that the binding sites of P450_{cam} and microsomal P450s are different enough that the product distributions of the hydroxylated metabolites are affected. While the product distribution may be different for the two isozymes, it is possible that the predicted stereoselectivity could be the same.

Our prediction of the absence of the C4'-OH metabolite could be especially significant in the assessment of toxic and teratogenic effects caused by VPA, since the formation of the 4-ene-VPA

product could proceed via H abstraction at either the C4 or C4' positions in the absence of steric constraints. It has been experimentally shown that it is the 4-ene-VPA metabolite that displays liver toxicity¹² and, independently, is known to be a teratogen.⁸ More specifically, it has recently been shown that the teratogenicity is due principally to the *S* stereoisomer of 4-ene-VPA.³⁹ If the C4'-OH is absent as a metabolite of P450, then the teratogenic *S* stereoisomer would not be formed from therapeutically administered VPA, providing an explanation for why metabolites of VPA are apparently not responsible for its teratogenicity.⁴⁰ Thus, knowledge of the steric interactions in the binding site of P450 should be useful in designing future drugs with lower toxicity and free of teratogenic consequences by exploiting the possible stereospecificity of P450 metabolism of substrates.

Experiments determining the identity and stereoselectivity of metabolites of VPA using P450_{cam} as the enzyme would test our predictions and guide future theoretical modeling efforts of mammalian cytochrome P450s. In addition, experimental determination of the stereospecificity of the hydroxylated products from the metabolism of VPA by both microsomal P450 and P450_{cam} would further serve as a test of our predicted stereoselectivity and lead to greater insights into the differences between the binding sites of mammalian P450s and P450_{cam} and their detailed interactions with substrates.

Acknowledgment. Support for this work from the Environmental Protection Agency Grant CR-816013-01-0 is gratefully acknowledged.

Registry No. VPA, 99-66-1; 4-ene-VPA, 1575-72-0; C3-OH, 58888-84-9; C4-OH, 60113-82-8; C5-OH, 53660-23-4; cytochrome P450, 9035-51-2; monooxygenase, 9038-14-6.

(38) Baillie, T., private communication.

(39) Nau, H.; Hauck, R.-S. *Toxicol. Lett.* **1989**, *49*, 41-48.

(40) Nau, H. *Fundam. Appl. Toxicol.* **1986**, *6*, 662-668.

Constructing a Molecular Model of the Interaction between Antithrombin III and a Potent Heparin Analogue

Peter D. J. Grootenhuys* and Constant A. A. van Boeckel*

Contribution from the Akzo Pharma Division, Organon Scientific Development Group, P.O. Box 20, 5340 BH Oss, The Netherlands. Received August 14, 1990

Abstract: Information about the antithrombin III-heparin interaction is deduced from the following: (i) structure-activity studies of various synthetic analogues of the antithrombin III binding pentasaccharide domain of heparin, which revealed that essential sulfate and carboxylate substituents are located at opposite sides of the pentasaccharide molecule; (ii) studies that designated the heparin-binding amino acid residues of antithrombin III; (iii) a molecular model of antithrombin III, constructed on the basis of the crystal structure of α 1-antitrypsin. From these studies it could be deduced that *both* the protein and the carbohydrate display an asymmetric assembly of essential interaction points. Docking trials indicated a single complex in which the interaction points are complementary. The latter complex was optimized by molecular dynamics simulations. The final model reveals, for the first time, how a well-defined region of a sulfated polysaccharide can interact specifically with a complementary binding site on a functional protein.

Although it has been recognized that interactions among sulfated polysaccharides (glycosaminoglycans) and proteins are involved in cellular adhesion and various physiological processes, only the heparin-antithrombin III (AT-III) system has been studied at the molecular level.¹ A major breakthrough was the finding that only part of the sulfated polysaccharides^{2,3} of the anticoagulant drug heparin displays high affinity to AT-III. Subsequently, it was discovered that this part of the heparin

polysaccharides contains a well-defined pentasaccharide region^{4,5} that specifically binds and activates the protease inhibitor AT-III.

(1) *Heparin, Chemical and Biological Properties, Clinical Applications*; Lane, D. A., Lindahl, V., Eds.; Edward Arnold: London, 1989.

(2) Lam, L. H.; Silbert, J. E.; Rosenberg, R. D. *Biochem. Biophys. Res. Commun.* **1976**, *69*, 570-577.

(3) Höök, M.; Björk, I.; Hopwood, J.; Lindahl, U. *FEBS Lett.* **1976**, *66*, 90-93.

(4) Choay, J.; Lormeau, J. C.; Petitou, M.; Sinay, P.; Fareed, J. *Ann. N.Y. Acad. Sci.* **1981**, *370*, 644-649.

* Author to whom correspondence should be addressed.